Applied Physics Letters

1550-nm InGaAsP multi-quantum-well structures selectively grown on v-groove-patterned SOI substrates

Cite as: Appl. Phys. Lett. **111**, 032105 (2017); https://doi.org/10.1063/1.4994318
Submitted: 24 April 2017 . Accepted: 04 July 2017 . Published Online: 18 July 2017

Ludovico Megalini, Bastien Bonef, Brian C. Cabinian, Hongwei Zhao, Aidan Taylor, James S. Speck, John E. Bowers, and Jonathan Klamkin

AIP Publishing

1550-nm InGaAsP multi-quantum-well structures selectively grown on v-groove-patterned SOI substrates

Ludovico Megalini,[1,a)] Bastien Bonef,[2] Brian C. Cabinian,[2] Hongwei Zhao,[1] Aidan Taylor,[2] James S. Speck,[2] John E. Bowers,[1,2] and Jonathan Klamkin[1]
[1]*Electrical and Computer Engineering Department, University of California, Santa Barbara, California 93106, USA*
[2]*Materials Department, University of California, Santa Barbara, California 93106, USA*

(Received 24 April 2017; accepted 4 July 2017; published online 18 July 2017)

We report direct growth of 1550-nm InGaAsP multi-quantum-well (MQW) structures in densely packed, smooth, highly crystalline, and millimeter-long InP nanoridges grown by metalorganic chemical vapor deposition on silicon-on-insulator (SOI) substrates. Aspect-ratio-trapping and selective area growth techniques were combined with a two-step growth process to obtain good material quality as revealed by photoluminescence, scanning electronic microscopy, and high-resolution X-ray diffraction characterization. Transmission electron microscopy images revealed sharp MQW/InP interfaces as well as thickness variation of the MQW layer. This was confirmed by atom probe tomography analysis, which also suggests homogenous incorporation of the various III-V elements of the MQW structure. This approach is suitable for the integration of InP-based nanoridges in the SOI platform for new classes of ultra-compact, low-power, nano-electronic, and photonic devices for future tele- and data-communications applications. *Published by AIP Publishing.*
[http://dx.doi.org/10.1063/1.4994318]

Semiconductor nanowires have attracted considerable attention for a wide variety of applications including optical data communications, quantum information, energy harvesting, and medical/biological diagnosis. In addition, if gain materials are incorporated, nanowires could be fabricated into nanolasers, and their reduced geometrical size can offer advantages compared to their equivalent bulk counterparts. Such advantages include higher density of states and consequently higher optical gain,[1,2] lower threshold current[3] and temperature sensitivity,[4] smaller linewidth, and higher modulation bandwidth.[5] Early reports described structures based on binary semiconductor nanowires covering the wavelength spectrum from the UV[6] to the near-infrared.[7] Nanowires fabricated from bulk III-V substrates and containing multi-quantum-well (MQW) structures[8] and quantum dots (QDs)[9] were also proposed to independently optimize both the gain medium and the optical cavity.

More recently, InGaAs MQW structures embedded in horizontal GaAs[10] and InP[11,12] nanowires were grown on patterned Si. Integrating these devices on Si by direct hetero-epitaxy is of great interest for silicon photonics and on-chip interconnect applications. Although flip-chip and wafer bonding techniques are currently more mature, monolithic solutions are preferred for large-scale manufacturing and to fabricate compact and complex photonic integrated circuits.[13] Direct growth of high-quality III-V materials on Si, however, poses extraordinary challenges due to the large difference in lattice constants, polarity, and thermal expansion coefficient of these crystals, which result in a high density of defects, including anti-phase boundaries, twins, stacking faults, and threading and misfit dislocations. These can strongly degrade the quality of the hetero-epitaxy and ultimately limit the performance and reliability of the devices. Metalorganic chemical vapor deposition (MOCVD) selective area growth (SAG) combined with aspect ratio trapping (ART) appears to be particularly promising to overcome these issues while producing high material quality on a large scale and with high yield. However, fabricating nanolasers grown on v-groove-patterned Si substrates [Fig. 1(a)] presents several difficulties that relate to the optical mode leakage into the thick Si substrate [Fig. 1(b)]. Etching the Si below the nanodevice, which is thus left suspended, adds further thermal, electrical injection, and mechanical stability problems.[14,15] By contrast, these issues are not present if the structure is grown on v-groove-patterned silicon-on-insulator (SOI) wafers [Fig. 1(c)].

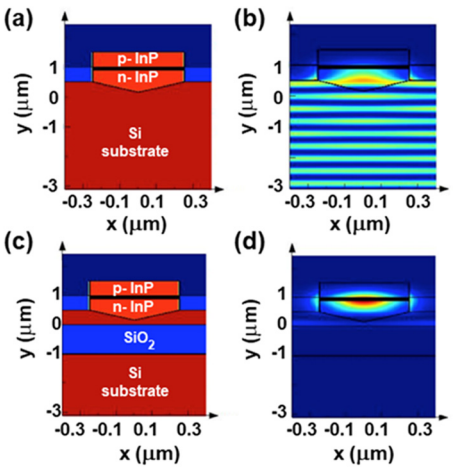

FIG. 1. (a) Schematic of nanolaser grown on v-groove-patterned Si substrate and (b) relative first TE mode profile showing high optical leakage into the Si substrate, (c) schematic of nanolaser grown on v-groove- patterned SOI substrate, and (d) relative first TE mode profile showing good confinement in the nanowire active region.

[a)]Email: megalini@engineering.ucsb.edu

The corresponding first TE mode [Fig. 1(d)] is sufficiently confined compared to the same device structure grown on a Si substrate (confinement factor of 13.4% on SOI compared to 1.2% on Si). Growing structures on SOI can therefore broaden the laser design space[16] and may also improve material quality by leveraging mechanical and thermal benefits.[17–21]

In this work, 1550-nm MQW structures in densely packed, smooth, highly crystalline, and millimeter-long horizontal InP nanoridges were grown by MOCVD on SOI substrates. The SOI has a thickness of 500 nm and is lightly p-type doped, and the buried oxide (BOX) layer has a thickness of 1 μm. After deposition of a 500-nm-thick SiO_2 film on the Si device layer by plasma-enhanced chemical vapor deposition (PECVD), 3-mm-long and 200-nm-wide 800-nm-pitch stripes oriented along the [110] direction were patterned by deep ultraviolet (DUV) lithography and etched by inductively coupled plasma etching (ICP) using conventional CF_4/CHF_3-based chemistry. The wafers were then diced to $2 \times 2\,cm^2$ pieces. Following RCA-1 cleaning, the Si device layer was etched with dilute potassium hydroxide (KOH) at 70 °C to form v-grooves and to expose the {111} Si surface for growth and to prevent the formation of anti-phase domain defects.[22] A small undercut formed at the Si/SiO_2 interface was found to be beneficial[23] [Fig. 2(a)] to capture most of the stacking faults propagating from the Si device layer into the III-V layer [Fig. 2(b)]. The Si native oxide was removed before growth by rapid immersion in buffered hydrofluoric (BHF) acid followed by annealing in the MOCVD chamber at 825 °C for 25 min in H_2 at 50 Torr. Trimethylindium (TMIn) and trimethylgallium (TMGa), Tertiarybutyl arsine (TBAs) and Tertiarybutyl phosphine (TBP) were used as group III and V precursors during the entire growth, Diethylzinc (DEZn) and Disilane (Si_2H_6) as p- and n-dopant sources, respectively. Two thin low-temperature nucleation layers (20 nm in total) of GaAs were deposited at 410 °C and at 430 °C with V/III ratios of 6 and 12, respectively, which in this surface-reaction limited regime were found to produce a thin and conformal layer on Si with very high selectivity between Si and SiO_2. A low-temperature InP nucleation layer was also deposited at 430 °C with a V/III ratio of 628; a high V/III ratio for InP has been suggested[24] to obtain full and uniform coverage of the trenches.[25] Next, two high-temperature, highly crystalline InP layers were deposited at 550 °C, and at 600 °C with V/III ratios of 40 and 89, respectively. Finally, 1550-nm InGaAsP quantum wells and barriers, followed by an InP layer 400 nm thick were grown, both at 650 °C. The growth rate of the high-temperature InP layers above and below the MQW structure was 3.72 A/s estimated from previous calibrations on planar InP substrates, the growth pressure was between 350- and 375 Torr for all layers. The as-grown InP horizontal nanowires were ~1.3 μm thick and exhibit a good height uniformity over a wide area [Fig. 2(c)] while demonstrating flat (001) and smooth (111) surfaces as observed in the plan-view scanning electron microscopy (SEM) images [Figs. 2(d) and 2(e)]. The high crystal quality of these structures was confirmed by high-resolution X-ray diffraction (XR-XRD) using a Philips PANalytical system operated at a voltage of 40 kV and a current of 45 mA. The ω-2θ scan around the (004) InP Bragg reflection clearly shows the InP peak at 31.54° along with the Si device layer at 34.43° and the Si substrate peak at 34.68° [Fig. 3(a)]. The angular separation of the two Si layers is unique to bonded wafers as it corresponds to the tilt between the layer and substrate Si planes,[26] and in fact, it is not seen in SIMOX (separation by implanted oxygen) wafers since in that case the two layers emerge from the same bulk crystal and thus are perfectly aligned.[27] The MQW manifest as a small hump on the left side of the InP peak and are more clearly visible in the (004) reciprocal space map (RSM) below the InP peak [Fig. 3(b)]. The layer appears to be under compressive strain, similarly to what is observed when the same layer is grown on a planar InP substrate. However, the typical strain-induced

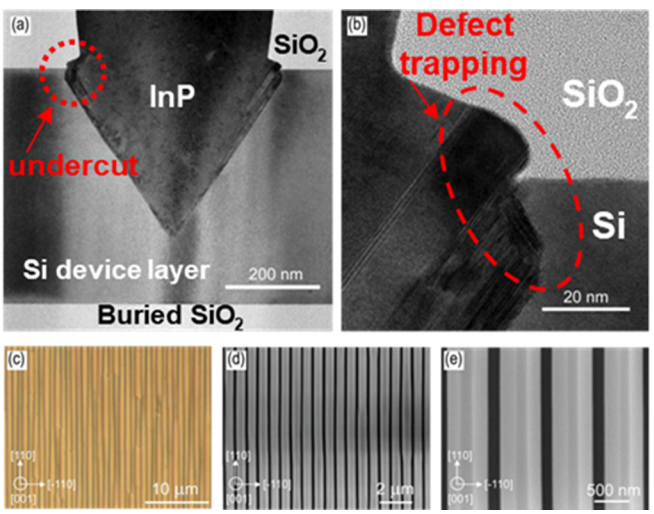

FIG. 2. (a) and (b) Cross-sectional HR-TEM images showing defects trapping by the Si undercuts, (c) Nomarski differential interference contrast (DIC), and (d) and (e) SEM plain-view images of the InP nanowires showing good height uniformity and surface morphology.

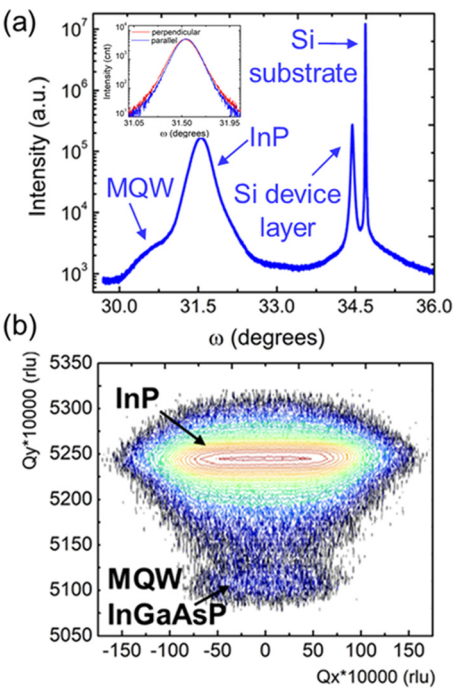

FIG. 3. (a) ω-2θ scan centered on (004) InP Bragg reflection showing the InP, Si-device layer and Si substrate peak, and (b) (004) InP ω-rocking curve scan along the parallel and perpendicular direction of the InP nanowires.

interference fringes occurring on planar growth are not clearly visible possibly because of the layer triangular shape and the different strain mechanism occurring in the patterned SOI substrates. This can also affect the direct gap energy.[28] Although interesting, the mechanism for the strain accommodation in this particular structure is not the scope of this letter. To further assess the quality of the InP layer, ω-rocking scans were performed across the (004) InP, and the FWHM was measured to be 633 arc sec and 688 arc sec when the line-focused x-ray beam was aligned parallel and perpendicular to the InP nanowires, respectively [Fig. 3(inset)]. These values are in the same range of similar InGaAs MQW in InP nanowires structures grown on Si[23,29] and indicate a slight unequal distribution of the defects along the [1-10] and [110] direction.

Figure 4 shows a strong room-temperature photoluminescence (PL) emission at 1555.7 nm emanating from the MQW structure under a laser pump power density of 20.5 W/cm^2. The measured PL FWHM is 135 nm. At lower pump power the spectrum was broader because at high excitation intensities the influence from defects is less pronounced due to saturation. Inhomogeneous spectrum shape broadening and changes in wavelength peak emission were also observed on different sample spots. These can be attributed to the relatively poor shape uniformity of the MQW layer observed over multiple fins as shown in the cross section FIB-SEM image of Fig. 5(a). The morphology of the nanowires was also investigated by cross-section transmission electron microscopy (TEM) analysis. The sample was imaged with a FEI Tecnai G2 Sphera operated at 200 kV in high resolution (HR) and bright field (BF) TEM modes. From cross-sectional HR-TEM images, the MQW and the p-InP layer appear free of any significant crystalline defects, which appear mostly localized within the first ~25 nm of the GaAs/InP layer and at the Si recess under the SiO_2. Figure 5(b) shows a BF-TEM image of a nanowire displaying a good and symmetric morphology. On this image the MQWs appear darker in color than the InP layers. The MQW appear thicker on the {001} surface compared to the {111} facets as observed on BF-TEM images of the {001} surface and the (11-1B) facet, respectively, displayed in Figs. 5(c) and 5(d). The distinction between QWs (lighter contrast) and barrier layers (darker contrast) can be clearly made both on the {111} facets and the {001} surface with well-defined interfaces. The MQW have different thicknesses as shown in Figs. 5(c) and 5(d), in particular, it was noticed that the thickness of both the barriers and wells decreased along the growth

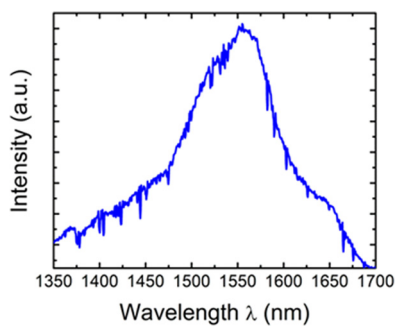

FIG. 4. PL emission showing emission at 1567 nm from the MQW structure inside the InP nanowires grown on the v-groove patterned SOI.

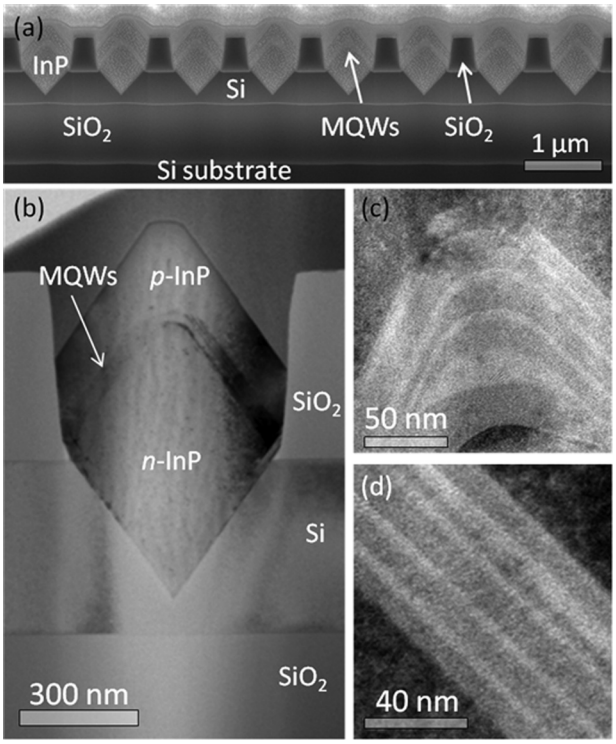

FIG. 5. (a) FIB-SEM Cross-section images of InP nanowires showing regular morphology. (b) BF-TEM image of a single nanowire with a good symmetry. BF-TEM images of the QWs and the barrier layers in (a) the (001) surface and (b) the {11-1B} facet. Dark colored layer is the barrier, light colored is quantum well.

direction as also reported in Ref. 10 for InGaAs MQW embedded in GaAs nanoridges. Little thickness fluctuations are observed between the (111B) and (11-1B) facets [Fig. 5(b)]. This trend was observed in all the nanowires imaged in TEM. The thickness variation result in a spectrum inhomogeneous broadening, which consequently would limit the gain of eventual final devices.[30] A more uniform QW thickness can be achieved by carefully adjusting the growth time of each QW as well as their position within the nanowire. Once all the growth parameters of the full stack are properly optimized, the growth preference towards the {001} surface would be desirable because the carriers of the MQW deposited along the {111} facets, if these are too thin, tend to be pushed up towards the In-rich flat central region.[31,32] This additional lateral quantum confinement can result in an increase of the radiative recombination, which in turn may potentially improve device performance.[33]

The quality of the MQW interfaces and the composition of each QW were evaluated by atom probe tomography (APT). This technique is preferred to secondary ion mass spectroscopy (SIMS) depth profiling because of the small size of the nanowires. An APT specimen was prepared with a FEI Helios 600 dual beam FIB instrument following the standard procedure with final FIB voltage down to 2 kV to minimize Ga induced damage.[34] The milling of the APT specimen was optimized to obtain a sharp tip extracted in a symmetric nanowire. APT analyses were performed with a Cameca 3000X HR Local Electrode Atom Probe (LEAP) operated in laser-pulse mode (13 ps pulse, 532 nm green laser, 10 μm laser spot size) with a sample base temperature

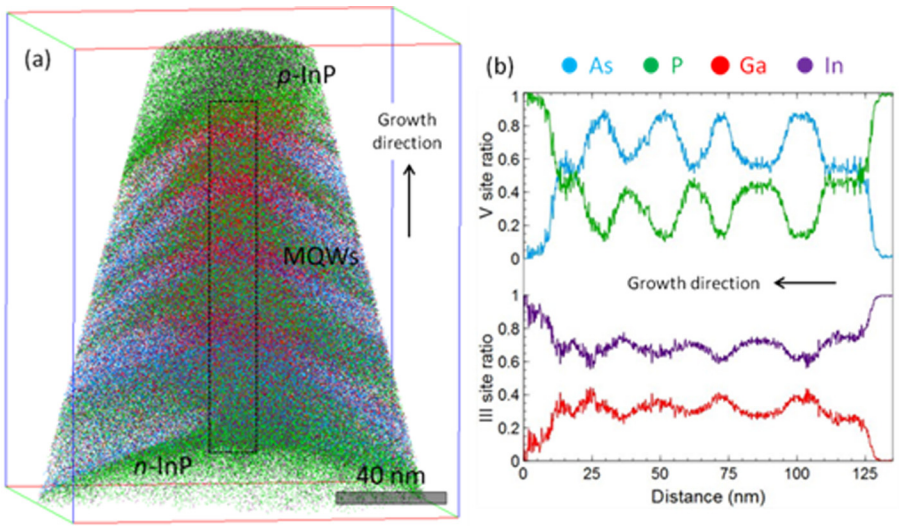

FIG. 6. (a) 3D reconstruction of the APT tip showing the MQW and III and V site atoms, and (b) relative composition profiles of $20 \times 20 \times 135\,\text{nm}^3$ sampling volume containing the QWs and along the growth direction.

of 40 K. The laser pulse energy was set to the minimum allowed value at 0.1 nJ. A detection rate of 0.005 atoms pulse^{-1} was set during the analysis. APT 3D reconstruction was carried out using the commercial software IVAS^{TM}. The reconstruction is optimized by using the SEM image of the tip as a reference.[35] Figure 6(a) shows a 3D reconstruction of the APT tip where the MQWs are clearly visible. The {001} surface and the {111} facets can be seen with the symmetry between the (111B) and the (11-1B) facets being respected. Both p- and n-InP doped layers can also be observed, and Si dopant ions could be seen in the APT mass spectrum. Zn signal which should be observed in mass ranges [32–35] and [64–70] in the APT mass spectrum was not detected probably because of its overlap in the APT mass spectrum with the thermal tails originating from the evaporation of P^+ at 31 amu and P^{2+} at 62 amu. The III-V elements concentration profile drawn with a moving step of 0.2 nm along a $20 \times 20 \times 135\,\text{nm}^3$ sampling volume extracted perpendicular to the MQW interfaces and along the growth direction is shown in Fig. 6(b). On this profile, the interfaces are sharp enough to make a clear distinction between the QWs and the barrier layers. It is however not possible to conclude on whether the bottom interfaces (QW on barrier) are sharper than the top interfaces (barrier on QW) as a clear trend is not observed. It is still worth noting that the bottom interface of the first buffer layer is sharper than the top interface of the last barrier layer where the diffusion of Ga and As is observed 10 nm in the p-doped InP layer. Compositions are calculated as III site and V site atomic fraction in the QWs and the barrier layers [i.e.,: In/(In + Ga), Ga/(In + Ga), P/(P + As), and As/(P + As)] and displayed in Table I. Ga and In fractions have little fluctuations between the wells and the barriers. The average values over the region of interest are 0.32 ± 0.01 and 0.68 ± 0.01, respectively, for Ga and In. In growth order, the peak As fractions in the QWs are 0.85 ± 0.01, 0.84 ± 0.01, 0.86 ± 0.01, and 0.83 ± 0.01. The As incorporation in the barrier layers is constant and around 0.56 ± 0.01. Using the model of Ref. 28, a structure with this composition grown on a planar InP substrate would yield a bandgap within 3% of the PL emission measured in this work. APT revealed that, despite the difficulty of growing the active region on non-planar feature,[36] a homogenous incorporation of the different elements can still be obtained between the QWs by properly selecting the growth parameters. In spite of the good top surface morphology of the InP nanowires, further improvement in material quality should be achieved for actual device fabrication.

TABLE I. III site and V site atomic fraction in the QWs and the barrier layers.

III and V site fraction	Ga	In	As	P
1st barrier	0.25	0.75	0.54	0.46
1st well	0.38	0.62	0.85	0.15
2nd barrier	0.28	0.72	0.55	0.45
2nd well	0.38	0.62	0.84	0.16
3rd barrier	0.30	0.70	0.56	0.44
3rd well	0.35	0.65	0.86	0.14
4th barrier	0.28	0.72	0.61	0.39
4th well	0.35	0.65	0.83	0.17
5th barrier	0.31	0.69	0.54	0.46

In conclusion, 1550-nm MQW structures on SOI substrates were grown by MOCVD using the ART technique and SAG. Special v-groove patterning of the Si device layer was used to trap most of the defects at the Si/SiO_2 interface, rendering the MQW and the upper III-V layers nearly defect free. Future work will focus on improving the epitaxial material quality, in particular, that of the MQW layers. Although SOI can provide a solution to the optical leakage loss of Si substrates, designing and fabricating nanolasers grown hetero-epitaxially remains challenging. In particular, it is not trivial to design a doping profile that can ensure good carrier injection and electrical contacts, while minimally disturbing the optical mode of the nanolaser. The presented approach, however, appears promising for new classes of ultra-small, low-power, nano-electronic and photonic devices on SOI for future tele- and data-communications applications.

This research was supported by the American Institute for Manufacturing (AIM) Integrated Photonics. A portion of this work was performed in the UCSB nanofabrication facility, part of the NSF NNIN network (ECS-0335765), as well as the UCSB CNSI and UCSB MRL, which are supported by the NSF MRSEC program (DMR1121053).

Funding for B. Bonef was provided by the Solid State Lighting & Energy Electronics Center.

[1]A. Yariv, "Scaling laws and minimum threshold currents for quantum-confined semiconductor lasers," Appl. Phys. Lett. **53**, 1033 (1988).
[2]E. Kapon, D. M. Hwang, M. Walther, R. Bhat, and N. G. Stoffel, "Two-dimensional quantum confinement in multiple quantum wire lasers grown by OMCVD on V-grooved substrates," Surf. Sci. **267**, 593 (1992).
[3]S. Simhony, E. Kapon, E. Colas, D. M. Hwang, N. G. Stoffel, and P. Worland, "Vertically stacked multiple-quantum-wire semiconductor diode lasers," Appl. Phys. Lett. **59**, 2225 (1991).
[4]Y. Arakawa and H. Sakaki, "Multidimensional quantum well laser and temperature dependence of its threshold current," Appl. Phys. Lett. **40**, 939 (1982).
[5]Y. Arakawa and A. Yariv, "Quantum well lasers-gain, spectra, dynamics," IEEE J. Quantum Electron. **22**, 1887 (1986).
[6]M. H. Huang, S. Mao, H. Feick, H. Yan, Y. Wu, H. Kind, E. Weber, R. Russo, and P. Yang, "Room-temperature ultraviolet nanowire nanolasers," Science **292**, 1897–1899 (2001).
[7]A. H. Chin, S. Vaddiraju, A. V. Maslov, C. Z. Ning, M. K. Sunkara, and M. Meyyappan, "Near-infrared semiconductor subwavelength-wire laser," Appl. Phys. Lett. **88**, 163115 (2006).
[8]F. Qian, Y. Li, S. Gradecak, H. Park, Y. Dong, Y. Ding, Z. L. Wang, and C. M. Lieber, "Multi-quantum-well nanowire heterostructures for wavelength-controlled lasers," Nat. Mater. **7**, 701–706 (2008).
[9]J. Tatebayashi, S. Kako, J. Ho, Y. Ota, S. Iwamoto, and Y. Arakawa, "Room-temperature lasing in a single nanowire with quantum dots," Nat. Photonics **9**, 501–505 (2015).
[10]B. Kunert, W. Guo, Y. Mols, B. Tian, Z. Wang, Y. Shi, D. Van Thourhout, M. Pantouvaki, J. Van Campenhout, R. Langer, and K. Barla, "III/V nano ridge structures for optical applications on patterned 300 mm silicon substrate," Appl. Phys. Lett. **109**, 091101 (2016).
[11]S. Li, X. Zhou, M. Li, X. Kong, J. Mi, M. Wang, W. Wang, and J. Pan, "Ridge InGaAs/InP multi-quantum-well selective growth in nanoscale trenches on Si (001) substrate," Appl. Phys. Lett. **108**, 021902 (2016).
[12]Y. Han, Q. Li, and K. M. Lau, "Highly ordered horizontal indium gallium arsenide/indium phosphide multi-quantum well in wire structure on (001) silicon substrates," J. Appl. Phys. **120**, 245701 (2016).
[13]B. Song, C. Stagarescu, S. Ristic, A. Behfar, and J. Klamkin, "3D integrated hybrid silicon laser," Opt. Express **24**(10), 10435–10444 (2016).
[14]B. Tian, Z. Wang, M. Pantouvaki, P. Absil, J. Van Campenhout, C. Merckling, and D. Van Thourhout, "Room temperature O-band DFB laser array directly grown on (001) silicon," Nano Lett. **17**(1), 559–564 (2017).
[15]Z. Wang, B. Tian, M. Pantouvaki, W. Guo, P. Absil, J. Van Campenhout, C. Merckling, and D. Van Thourhout, "Room-temperature InP distributed feedback laser array directly grown on silicon," Nat. Photonics **9**, 837–842 (2015).
[16]H. Kim, A. C. Farrell, P. Senanayake, W. J. Lee, and D. L. Huffaker, "Monolithically integrated InGaAs nanowires on 3D structured silicon-on-insulator as a new platform for full optical links," Nano Lett. **16**(3), 1833–1839 (2016).
[17]S. J. Pearton, S. M. Vernon, K. T. Short, J. M. Brown, C. R. Abernathy, R. Caruso, S. N. G. Chu, V. E. Haven, and S. N. Bunker, "Characterization of GaAs grown by metalorganic chemical vapor deposition on Si-on-insulator," Appl. Phys. Lett. **51**, 1188 (1987).
[18]N. H. Karam, V. Haven, S. M. Vernon, F. Namavar, N. El-Masry, and M. M. Al-Jassim, *Growth and Characterization of InP/GaAs on SOI by MOCVD* (Mater. Res. Soc. Symp. Proc., 1990), Vol. 198, pp. 247–252.
[19]M. L. Seaford, D. H. Tomich, K. G. Eyink, L. Grazulis, K. Mahalingham, Z. Yang, and W. I. Wang, "Comparison of GaAs grown on standard Si (511) and compliant SOI (511)," J. Electron. Mater. **29**(7), 906–908 (2000).
[20]T. P. Humphreys, C. J. Miner, J. B. Posthill, K. Das, M. K. Summerville, R. J. Nemanich, C. A. Sukow, and N. R. Parikh, "Heteroepitaxial growth and characterization of GaAs on silicon-on-sapphire and sapphire substrates," Appl. Phys. Lett. **54**, 1687 (1989).
[21]L. S. Wang, S. Tripathy, S. J. Chua, and K. Y. Zang, "Multi-quantum-well structures on (111)-oriented bonded silicon-on-insulator substrates," Appl. Phys. Lett. **87**, 111908 (2005).
[22]M. Paladugu, C. Merckling, R. Loo, O. Richard, H. Bender, J. Dekoster, W. Vandervorst, M. Caymax, and M. Heyns, "Site selective integration of III–V materials on Si for nanoscale logic and photonic devices," Cryst. Growth Des. **12**(10), 4696–4702 (2012).
[23]Y. Han, Q. Li, S. Chang, W. Hsu, and K. M. Lau, "Growing InGaAs quasi-quantum wires inside semi-rhombic shaped planar InP nanowires on exact (001) silicon," Appl. Phys. Lett. **120**, 245701 (2016).
[24]C. Merckling, N. Waldron, S. Jiang, W. Guo, N. Collaert, M. Caymax, E. Vancoille, K. Barla, A. Thean, M. Heyns, and W. Vandervorst, "Heteroepitaxy of InP on Si(001) by selective-area metal organic vapor-phase epitaxy in sub-50 nm width trenches: The role of the nucleation layer and the recess engineering," J. Appl. Phys. **115**, 023710 (2014).
[25]S. Jiang, C. Merckling, A. Moussa, W. Guo, N. Waldron, M. Caymax, W. Vandervorst, M. Seefeldt, and M. Heyns, "Influence of trench width on III-V nucleation during InP selective area growth on patterned Si(001) substrates," ECS Trans. **64**(6), 501–511 (2014).
[26]G. M. Cohen, P. M. Mooney, E. C. Jones, K. K. Chan, P. M. Solomon, and H.-S. P. Wong, "Characterization of the silicon on insulator film in bonded wafers by high resolution x-ray diffraction," Appl. Phys. Lett. **75**, 787 (1999).
[27]V. Antonova, V. P. Popov, J. Bak-Misiuk, and J. Z. Domagala, "Characterization of silicon-on-insulator structures by high-resolution X-ray diffraction," J. Electrochem. Soc. **149**(8), G490–G493 (2002).
[28]J. R. Flemish, H. Shen, K. A. Jones, M. Dutta, and V. S. Ban, "Determination of the composition of strained InGaAsP layers on InP substrates using photoreflectance and double-crystal x-ray diffractometry," J. Appl. Phys. **70**, 2152 (1991).
[29]Q. Li, K. W. Ng, and K. M. Lau, "Growing antiphase-domain-free GaAs thin films out of highly ordered planar nanowire arrays on exact (001) silicon," Appl. Phys. Lett. **106**, 072105 (2015).
[30]Z. Xin and H. N. Rutt, "Effect of inhomogeneity on quantum well far infrared lasers," J. Appl. Phys. **83**, 1491 (1998).
[31]G. Biasiol, A. Gustafsson, K. Leifer, and E. Kapon, "Mechanisms of self-ordering in nonplanar epitaxy of semiconductor nanostructures," Phys. Rev. B **65**, 205306 (2002).
[32]T. Schrimpf, P. Bönsch, D. Wüllner, H. H. Wehmann, A. Schlachetzki, F. Bertram, T. Riemann, and J. Christen, "InGaAs quantum wires and wells on V-grooved InP substrates," J. Appl. Phys. **86**, 5207 (1999).
[33]C. Constantin, E. Martinet, F. Lelarge, K. Leifer, A. Rudra, and E. Kapon, "Influence of strain and quantum confinement on the optical properties of InGaAs/GaAs V-groove quantum wires," J. Appl. Phys. **88**, 141 (2000).
[34]K. Thompson, D. Lawrence, D. J. Larson, J. D. Olson, T. F. Kelly, and B. Gorman, "*In situ* site-specific specimen preparation for atom probe tomography," Ultramicroscopy **107**, 131–139 (2007).
[35]F. Vurpillot, B. Gault, B. P. Geiser, and D. J. Larson, "Reconstructing atom probe data: A review," Ultramicroscopy **132**, 19–30 (2013).
[36]R. Bath, "Non-planar and masked-area epitaxy by organometallic chemical vapour deposition," Semicond. Sci. Technol. **8**, 984–993 (1993).